

Yb-Doped Cs₂AgInCl₆ Double Perovskite Microcrystals and Nanocrystals

A Thesis submitted to

Indian Institute of Science Education and Research (IISER), Pune

in partial fulfillment of the requirements for the

BS-MS Dual Degree Programme

By

Yogesh Mahor

(Reg. #20141021)

Under the Supervision of

Dr. Angshuman Nag

Assistant professor, Department of Chemistry



Indian Institute of Science Education and Research(IISER), Pune

Dr. Homi Bhabha Road, Pashan, Pune 411008, INDIA.

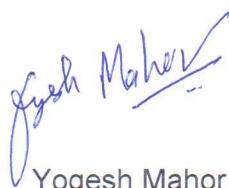
March, 2019

Certificate

This is to certify that this dissertation entitled "***Yb-Doped Cs₂AgInCl₆ Double Perovskite Microcrystals and Nanocrystals***" towards the partial fulfilment of the BSMS dual degree programme at the Indian Institute of Science Education and Research, Pune represents study/work carried out by **Yogesh Mahor** at IISER Pune under the supervision of **Dr. Angshuman Nag**, Assistant professor, Department of Chemistry, IISER Pune during the academic year 2018-19.

Date: 20th March, 2019

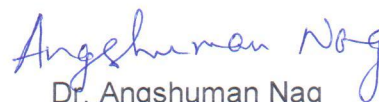
Place: Pune (Maharashtra)



Yogesh Mahor

5th year BSMS student

IISER Pune



Dr. Angshuman Nag

Assistant Professor

Department of Chemistry

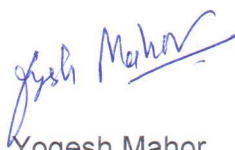
IISER Pune

Declaration

I hereby declare that the matter embodied in the report entitled "***Yb-Doped Cs₂AgInCl₆ Double Perovskite Microcrystals and Nanocrystals***" are the results of the work carried out by me at the Department of Chemistry, IISER Pune, under the supervision of **Dr. Angshuman Nag** and the same has not been submitted elsewhere for any other degree.

Date: 20th March, 2019


Place: Pune (Maharashtra)



Yogesh Mahor

5th year BSMS student

IISER Pune



Dr. Angshuman Nag

Assistant Professor

Department of Chemistry

IISER Pune

Acknowledgements

Firstly, I would like to express my sincere gratitude to my supervisor **Dr. Angshuman Nag** sir for his continuous support, guidance, motivation, enthusiasm and immense knowledge helped me successfully carried out this MS thesis. It would never have been possible for me to complete this work without his guidance and direction. His unwavering enthusiasm towards research kept me constantly engaged in my research and his personal generosity helped make my time enjoyable.

I am grateful to my thesis advisory committee member **Dr. Sujit k. Ghosh** for his guidance and helpful discussion during mid-sem presentation, which enabled me to make necessary improvements.

My special thanks go to former Director of IISER-Pune **Prof. K. N. Ganesh** and new Director of IISER-Pune **Prof. Jayant B. Udgaonkar** for providing an opportunity to carrying out this research work.

My appreciation also extends to all the faculty members in the IISER-Pune for teaching me various courses especially chemistry.

I would like to thank my astoundingly supporting lab members Wasim, Vikash, Tariq, Bharat, Abhishek, Habib, Rayan. It was always a pleasure coming to work every day with such lovely and engaging people. My deep gratitude goes for Wasim who expertly guided me throughout my fifth-year project and shared happiest moments, ups, downs and joy with me.

Heartfelt thanks to all my friends and my teammates who made IISER Pune experience special, in particular, Devendra, Sambit, Rajat, Sunil, Satendra, Harsha, Alok, Prashant, Vamshi, Rajat sonkar, Krishnendu, ashwini and priya batra for their great support especially during fifth year.

I am truly grateful to my grandparents, my parents, sister, brother and my inspiration Bhupesh chacha for their immense love and care.

I acknowledge SAIF-IIT Bombay and Dr. Gyana Ranjan's lab at IISER Pune for ICP-AES and ICP-MS analysis respectively. I acknowledge Dr. Pramod Pillai's Lab at IISER Pune for diffused reflectance spectroscopy measurements and Prof. JK's Lab at IISER Pune for TGA measurements. I also acknowledge IISER Pune for student fellowship.

Table of Contents

Abstract.....	9
Introduction	10
1. Yb-doped Cs₂AgInCl₆ Double Perovskite Microcrystals.	
1.1 Methods	13
1.1.1 Chemicals	13
1.1.2 Synthesis of Yb-Doped Cs ₂ AgInCl ₆ Microcrystals	13
1.1.3 Characterizations	14
1.1.3.1 Inductively coupled plasma- atomic emission spectroscopy (ICP-AES).....	14
1.1.3.2 Field emission scanning electron microscopy (FESEM).....	14
1.1.3.3 X-ray diffraction (XRD)	14
1.1.3.4 Thermogravimetric analysis (TGA)	15
1.1.3.5 UV-Vis-NIR Diffused reflectance spectroscopy).....	15
1.1.3.6 Steady-state Photoluminescence spectroscopy and Photoluminescence decay dynamics.....	15
1.2 Results and Discussion	16
1.2.1 Structure and Morphology of Yb-doped Cs ₂ AgInCl ₆ Microcrystals.....	16
1.2.2 Optical properties of Yb-doped Cs ₂ AgInCl ₆ Microcrystals.....	18
1.2.3 Stability of Yb-doped Cs ₂ AgInCl ₆ Microcrystals.....	20
1.3 Conclusions.....	21
2. Yb-doped Cs₂AgInCl₆ Double Perovskite Nanocrystals.	
2.1 Methods	23
2.1.1 Chemicals	23
2.1.2 Cesium Oleate Preparation.....	23
2.1.3 Synthesis of Yb-doped Cs ₂ AgInCl ₆ Nanocrystals.....	23
2.1.4 Characterizations	24
2.1.4.1 Inductively coupled plasma Mass spectroscopy (ICP-MS).....	24
2.1.4.2 X-ray diffraction (XRD)	24

2.1.4.3	Transmission electron microscopy and high-resolution.....	24
2.1.4.4	UV-Vis spectroscopy.....	25
2.1.4.5	Steady-state Photoluminescence spectroscopy and Photoluminescence decay dynamics.....	25
2.2	Results and Discussion	25
2.2.1	Structure and Morphology of Yb-doped Cs ₂ AgInCl ₆ Nanocrystals.....	25
2.2.2	Optical properties of Yb-doped Cs ₂ AgInCl ₆ Nanocrystals.....	28
2.3	Conclusions.....	29
	References.....	30

List of Figures

1. Transformation of lead halide perovskites to Double Perovskite.....	11
2. Schematic presentation Yb-doped Cs ₂ AgInCl ₆ Double Perovskite microcrystals.....	13
3. Morphology of x% Yb-doped Cs ₂ AgInCl ₆ Double Perovskite microcrystals.....	17
4. Structure of x% Yb-doped Cs ₂ AgInCl ₆ Double Perovskite microcrystals.....	18
5. Optical properties of x% Yb-doped Cs ₂ AgInCl ₆ Double Perovskite microcrystals.....	19
6. Stability Studies:	
a) X-ray diffraction data and b) thermogravimetric analysis data.....	20
7. Photoluminescence spectra at different time interval.....	21
8. Transmission Electron Microscopy and High Resolution Transmission Electron Microscopy images of Yb-doped Cs ₂ AgInCl ₆ nanocrystals.....	26
9. Size distribution histogram.....	27
10. X-ray diffraction patterns of undoped and Yb-doped nanocrystals.....	27
11. Optical properties of undoped and Yb-doped Cs ₂ AgInCl ₆ nanocrystals.....	28
12. Photoluminescence decay dynamics of Yb-emission collected at 996 nm.....	29

List of Table

1. Comparison of Yb concentration added in the reaction mixture with that found in the product.....	16
--	----

Abstract:

Lead halide perovskites (LHPs) is the class of semiconductor which shows enormous promise for photovoltaics (PVs) and light emitting diodes (LEDs) as they have excellent and easily tuneable optical properties. Having all those remarkable properties, they still suffer from lead toxicity and stability in ambient conditions. Due to which, their commercial use is difficult. An enormous amount of research has been going on by different research groups in search of lead free halide perovskite. They have come up with lead free double perovskites (DPs), and $\text{Cs}_2\text{AgInCl}_6$ DP is one of them. It has a direct band gap, and are stable and environmentally benign material with 3D perovskite structure. However, the band gap of these material is large (~ 3.3 eV) and so not desirable for optoelectronic applications. One way to achieve typical functionality is by doping optically active metal ions in the lattice of DPs. In this thesis, we show the synthesis and characterization of Ytterbium (Yb) doped $\text{Cs}_2\text{AgInCl}_6$ DPs. Doping of Yb metal ion provides the optical functionality in near infrared region (NIR). We have achieved the doping of Yb in microcrystals as well as colloidal nanocrystals of $\text{Cs}_2\text{AgInCl}_6$ DPs. Our Yb-doped $\text{Cs}_2\text{AgInCl}_6$ DPs show narrow NIR emission (~ 994 nm, 1.24 eV) by converting UV light absorbed by the host. These Yb-doped $\text{Cs}_2\text{AgInCl}_6$ DPs have millisecond range lifetime corresponding to $^2\text{F}_{5/2} \rightarrow ^2\text{F}_{7/2}$ transition of Yb^{3+} f electrons. One of the unique feature of these Yb-doped $\text{Cs}_2\text{AgInCl}_6$ DPs is that they do not suffer from self-absorption. Due to that they can emit pure NIR light and can be used in NIR light emitting diodes.

Major part of the work presented here has been submitted for research publication with following details. **Mahor, Y.**; Mir, W. J.; Nag, A. “*Synthesis and Near Infrared Emission of Yb Doped $\text{Cs}_2\text{AgInCl}_6$ Double Perovskite Microcrystals and Nanocrystals*”, **2019**, *submitted*.

INTRODUCTION

Lead halide perovskite (LHPs) of general formula $APbX_3$ (where $A = CH_3NH_3^+$, $CH_5N_2^+$; $X = Cl^-, Br^-, I^-$) have attracted enormous attention in the recent years as they show outstanding optoelectronic and optical properties.¹⁻³ Owing all these properties, LHPs are employed in various devices like solar cell, light emitting diodes (LEDs) and photodetectors.⁴⁻¹³ Despite all the excellent properties LHPs suffer from thermal and moisture instability and lead toxicity.¹⁴⁻¹⁶ A good amount of research has been involved in resolving these issues without sacrificing the key features of LHPs. Thermal stability are significantly improved by going from hybrid organic LHPs to all inorganic LHPs (A cation = Cs^+). However, there is another major issue to tackle, which is lead toxicity. For commercialization of electronic devices, toxic metals used in the devices should be within the non-hazardous limit. Encapsulation of LHPs in devices may solve the toxicity issue but that also increases the production cost as well as long term problem of lead toxicity still remains.

Researchers are trying to replace the B-site cation (Pb^{2+}) with homovalent cations such as Sn^{2+} and Ge^{2+} to mimic the properties of LHPs.¹⁷⁻²⁰ However, these homovalent cations easily goes to the more stable oxidation state (+4). This interrupt the 3D framework of the perovskite structure by making cation vacancy. Similarly, replacing Pb^{2+} with other cations like Sb^{3+} , Tl^+ and Bi^{3+} also led to break down of 3D network of the perovskite structure.²¹⁻²³ Therefore, they show poor optoelectronic properties. In recent year, research groups are trying to come up with alternative class of materials called metal halide double perovskite (DPs). DPs have the general formula of $A_2B^I B^{III} X_6$ ($A = Cs^+$, $B^I = Cu^+, Na^+, Ag^+, In^+$ and $B^{III} = Bi^{3+}, In^{3+}, Sb^{3+}, Ga^{3+}$).²⁴⁻³⁰ In designing of DPs, two of Pb^{2+} ions in $A_2Pb_2X_6$ unit have been replaced with one monovalent metal ion (M^+) and trivalent metal ion (M^{3+}). This combination of metal ions maintains the charge neutrality to get 3D halide double perovskite structure as represented in figure 1. $Cs_2AgBiCl_6$ and $Cs_2AgBiBr_6$ have band gap values of 2.77 eV and 2.19 eV respectively,^{31, 32} has been extensively studied.

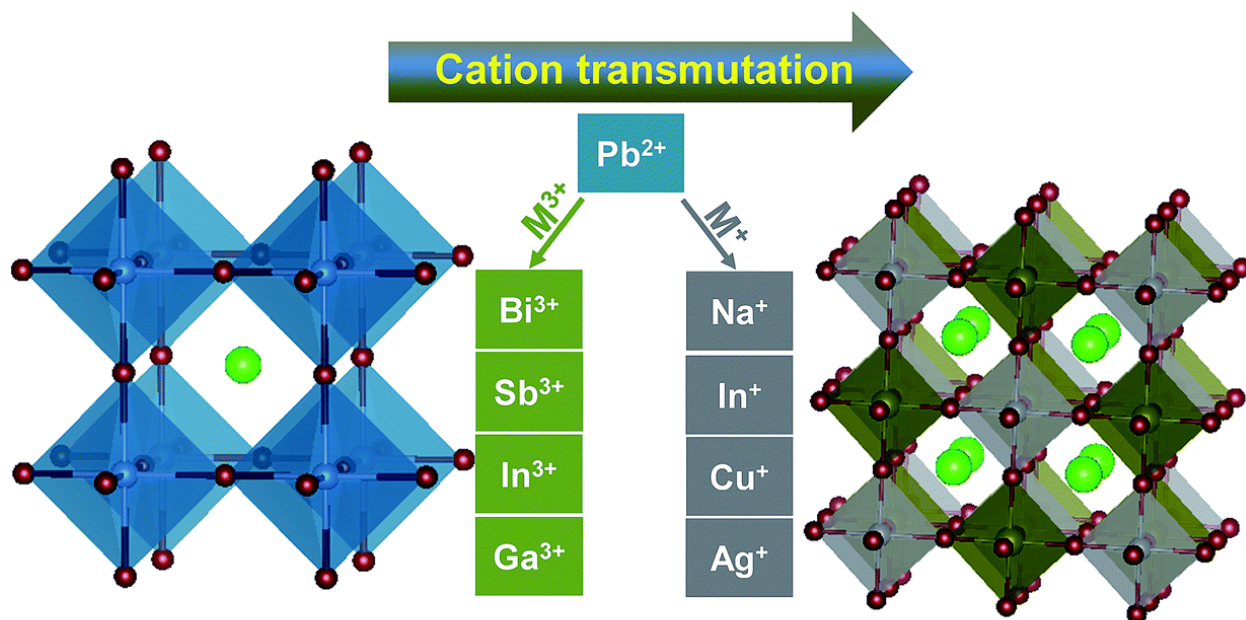


Figure 1: Transformation of lead halide perovskites to halide DPs by replacement of two Pb^{2+} cations with M^{3+} and M^{+} cations each. (Taken from ref. 29 with permission, Copyright 2018, Royal society of Chemistry).

These Bi-based DPs have wide bandgaps, and therefore not recommended for thin film solar cell and LEDs. In addition $\text{Cs}_2\text{AgBiBr}_6$ has indirect band gap with poor absorption coefficient. In difference $\text{Cs}_2\text{AgInCl}_6$ halide DPs has direct band gap and stable in ambient conditions.^{24-26, 30} The flat valence band maximum (VBM) is composed of Ag $4d$ and Cl $3p$ and conduction band minimum (CBM) is originating from delocalized In $5s$ states.³³ But the optical band gap of $\text{Cs}_2\text{AgInCl}_6$ DP is wide band gap (~ 3.3 eV)²⁵ in UV-region therefore does not show absorption and emission in the Vis-NIR region making it optoelectronically inactive in this popular region. Recent reports by Nandha et al³⁴ and Locardi et al³⁵ modulated optical properties of bulk and nanocrystals $\text{Cs}_2\text{AgInCl}_6$ respectively, by doping Mn^{2+} that emit orange coloured light. In this work, we have introduced the optical functionality in the NIR region by doping Yb^{3+} ions in the $\text{Cs}_2\text{AgInCl}_6$ DP.

Attempts has been done earlier for doping of Yb^{3+} ions in II-VI (CdSe, CdTe etc) and III-V (InP, GaAs etc) semiconductors.³⁶⁻³⁸ Doping of trivalent lanthanide (as Yb^{3+}) is not achieved in the lattice of the those crystals as trivalent lanthanide (Ln^{3+} and Yb^{3+}) tends

to prefer octahedral coordination over tetrahedral coordination of II-VI and III-V semiconductors. In last few year Yb doping in LHPs has gain a huge attention as these LHPs offer octahedral coordination sites for Ln^{3+} .³⁹⁻⁴² Just like APbX_3 , DPs also have those octahedral sites. We opted for Yb^{3+} over other lanthanide metal ions because Yb^{3+} metal ion involves only two energy states ($^2\text{F}_{5/2}$ and $^2\text{F}_{7/2}$). These two f states are separated by energy gap of 1.24 eV (~992 nm) falling into narrow NIR region.⁴³ This simplest f -electronic structure of Yb^{3+} minimizes non-radiative energy losses compared to other Ln^{3+} which typically have more than two valence f -electronic states.

This thesis is divided into two chapters. In first chapter, we will discussed the synthesis and characterization of microcrystals of Yb-Doped $\text{Cs}_2\text{AgInCl}_6$. In chapter 2, we will discuss the synthesis and characterization of nanocrystals of Yb-Doped $\text{Cs}_2\text{AgInCl}_6$.

Chapter 1: Yb-doped Cs₂AgInCl₆ Microcrystals

1.1 METHODS

1.1.1 Chemicals:

Hydrochloric acid (HCl, 37 wt %), cesium chloride (CsCl, 99.9%), indium (III) chloride (InCl₃, anhydrous powder, ≥99.999%), silver chloride (AgCl, 99.999%), are purchased from Sigma Aldrich Chemicals. Ytterbium chloride (YbCl₃, Ultra dry, ≥ 99%) is purchased from Alfa Aesar. All the precursors were used without any further purification.

1.1.2 Synthesis of Yb-doped Cs₂AgInCl₆ Microcrystals:

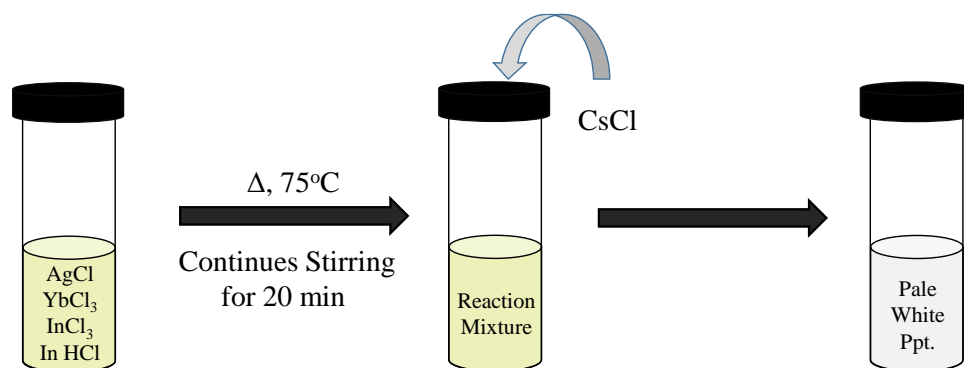


Figure 2: Schematic presentation Yb-doped Cs₂AgInCl₆ microcrystals

Synthesis of Yb-doped Cs₂AgInCl₆ microcrystals is developed based on the reported synthesis of undoped Cs₂AgInCl₆ microcrystals.³⁴ The reaction (figure 2) is carried out in a vial under ambient atmosphere involving acid precipitation of the product at ~75 °C. Typically, 0.5 mmol AgCl, 0.5 mmol InCl₃, different amounts (0.1 mmol, 0.2 mmol, 0.5 mmol and 1 mmol) of YbCl₃ and 4 mL HCl are taken in a 20 mL glass vial. The reaction mixture is kept for heating at 75 °C over a heating plate under vigorous stirring. After 20 minutes of heating, the reaction is initiated by adding 1 mmol CsCl. An immediate pale white precipitate appears and the reaction mixture is left on a heating plate for another 20 minutes under continuous stirring for completion of the reaction. The precipitate is filtered out and washed with ethanol three times, dried in oven (~110 °C) for 10 minutes and final powder is stored in a vial for further characterization.

1.1.3 Characterizations:

1.1.3.1 Inductively coupled plasma- atomic emission spectroscopy (ICP-AES):

This technique is involved in determining the elemental composition of the sample. In ICP-AES, the sample is excited by high electron density and high temperature argon plasma. When this excited sample is relaxed in there low energy states they emit element specific electromagnetic radiation (wavelengths). All emitted wavelengths from different elements simultaneously collected by the detector. Based on the intensity of different wavelengths and calibrated plot content of the element is determined.

To determine the doping percentage ICP-AES analysis has been carried out using ARCOS simultaneous ICP spectrometer, SPECTRO Analytical Instruments GmbH, Germany. All the samples were prepared in 2% HNO₃. The concentration of each sample was kept ~10 ppm. In the case of the dopant element, the contraction was maintained to 100 ppm and normalized to by the factor of 10.

1.1.3.2 Field emission scanning electron microscopy (FESEM):

FESEM technique provides information about size, shape and surface morphology and compositions of the compound. It has higher resolution and greater energy rang than convencinal SEM. In FESEM, Field emission gun is used as a electron source. Which provied the greater spatial resolution and low potential. FESEM images are taken with Zeiss Ultra Plus Field Emission SEM instrument. Samples were mounted on individual substrate holders using carbon tape and dried under vacuum for about 20 min before recording images.

1.1.3.2 X-ray diffraction (XRD):

X-ray diffraction is the technique which provide the information about crystal structure, size of the crystals, composition of crystals and lattice parameters. It work on the principal of constructive interference of the X-ray from the periodic arrangements of particles in crystal. These constructive interference occur because of the Wulff–Bragg's conditions.

$$2d \sin\theta = n\lambda$$

Where d is interplaner distance in crystals, θ is angle of diffraction of X-ray and λ is wavelength of incident X-ray.

XRD patterns was recorded using a Bruker D8 Advance X-ray diffraction (XRD) machine equipped with Cu K α (1.54 Å) radiation. All samples are evenly spered on glass slide to record XRD pattern.

1.1.3.3 Thermogravimetric analysis (TGA):

Thermogravimetric analysis is the technique to determine the thermal decomposition of the compound and phase change on the crystalline material. Weight loss of the samples are measured as function of temperature and time. TGA data are recorded using Perkin Elmer STA 6000 for about 3 mg of powder samples.

1.1.3.4 UV-Vis-NIR Diffused reflectance spectroscopy:

Diffused reflectance spectroscopy helps to record reflectance on the materials. Light is easily transmitted with much scattering in liquid samples. But in case of power samples light is tense to scatter in all the directions. Because of which be lost information. To convert reflectance in to absorbance using Kubelka-Munk function⁴⁵ defined as.

$$F(R) = (1 - R)^2 / 2R = \alpha/S$$

Where R is reflection, α is absorbance coefficient and S is scattering coefficient.

Diffused reflectance spectra of microcrystalline powders in UV-visible-NIR region are recorded using a SHIMADZU UV-3600 plus UV-Vis-NIR spectrophotometer.

1.1.3.5 Steady-state PL spectroscopy and PL decay dynamics:

Photoluminescence (PL) is the emission of light when excited electron relaxes from excited state to ground state by radiative emission of light. The emitted light have lower in energy compare to absorbed light. Samples has been excited by using steady state Xenon lamp and steady-state PL and PL excitation spectra was obtained. In case PL decay dynamics, excitation of the sample was done by using microsecond flash lamp. In decay dynamics time correlated single photon counting are measured. All the

measurements (steady-state PL, PLE and PL decay) was performed by using Edinburgh FLS 980 (Edinburgh Instruments).

To obtain the steady-state PL, PLE and PL decay spectra power sample was evenly spread on a quartz substrate.

1.2 RESULTS AND DISCUSSION:

1.2.1 Structure and Morphology of Yb-doped Cs₂AgInCl₆ Microcrystals

ICP-AES was employed to obtain Yb concentration in the final product and data are summarized in Table 1. In spite of using large amount of Yb, 9% to 50% of the total cation precursors ($[Yb] / ([Ag] + [In] + [Yb])$), the amount Yb in the product (Yb-doped Cs₂AgInCl₆ microcrystals) are found to be only in the range of 0.06% to 1.58%. These results suggest poor Yb-doping tendency in Cs₂AgInCl₆ microcrystals within our reaction conditions. Hereafter, we mention the Yb concentration obtained from ICP-AES analysis of the product throughout the chapter.

Table 1: Comparison of Yb concentration added in the reaction mixture with that found in the product. % is Yb is calculated following the equation $\{[Yb] / ([Ag] + [In] + [Yb])\} \times 100$.

Yb-doped Cs ₂ AgInCl ₆ microcrystals	
%Yb precursor taken	%Yb in product
9	0.06
16	0.25
33	0.96
50	1.58

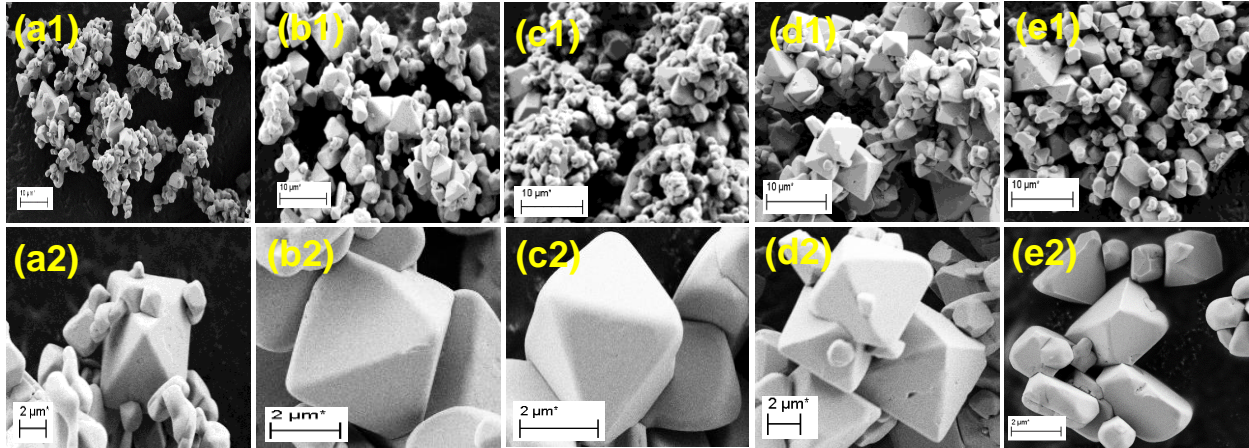


Figure 3: Morphology of x% Yb-doped $\text{Cs}_2\text{AgInCl}_6$ DP microcrystals. FESEM images of 0% (a1-a2), 0.06% (b1-b2), 0.25% (c1-c2), 0.96% (d1-d2), and 1.58% Yb (e1-e2) doped $\text{Cs}_2\text{AgInCl}_6$ microcrystals showing multifaceted growth.

FESEM images in Figure 3 show micrometre sized crystals with multifaceted growth of undoped and Yb-doped $\text{Cs}_2\text{AgInCl}_6$. The size ($\sim 5 \mu\text{m}$) and morphology remains similar for all samples with various Yb dopant percentages in the range of 0.06 to 1.58% Yb. To confirm the crystalline nature, we collected powder XRD patterns with varying Yb concentrations of samples as shown in Figure 4c. XRD pattern of the undoped sample match with prior report for cubic phase (elpasolite structure) of $\text{Cs}_2\text{AgInCl}_6$ DP.²⁴ Ag and In both occupy octahedral voids in alternating pattern forming 3D arrangement of AgCl_6 and InCl_6 , and Cs^+ is at cuboctahedral site (see Figure 4a & 4b). With increase in Yb doping concentrations, no additional impurity peak appears and the XRD patterns of all the samples are similar. These results confirm that the addition of Yb precursors in the reaction mixture do not produce any crystalline impurity phase. XRD peaks (see Figure 2(d) for $2\theta \sim 24.2^\circ$) do not exhibit systematic shift in 2θ values with Yb doping, probably because of the small ($\sim 1\%$) dopant concentrations. Yb^{3+} with ionic radii 0.86 \AA may replace In^{3+} (0.8 \AA), or Ag^+ (1.15 \AA) or both partially.⁴⁴ Yb^{3+} replacing In^{3+} is an isovalent substitution and both have nearly similar radii unlike Ag^+ , but, Ag^+ substitution may also occur with the formation of charged defects. Our present XRD studies are not sufficient to conclude whether Yb incorporation is taking place at In^{3+} site or Ag^+ site or at both sites.

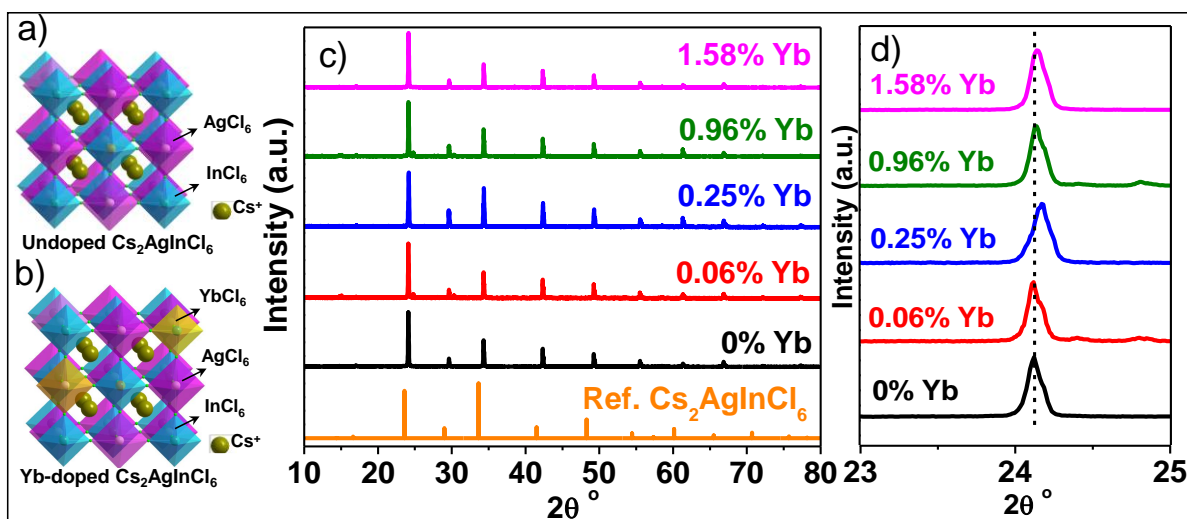


Figure 4: Structure of x% Yb-doped $\text{Cs}_2\text{AgInCl}_6$ DP microcrystals. (a) & (b) Schematics of Undoped and Yb-doped $\text{Cs}_2\text{AgInCl}_6$ DP with corner shared octahedra to form 3D perovskite structure similar to APbX_3 perovskite respectively. (c) XRD patterns of x% Yb-doped $\text{Cs}_2\text{AgInCl}_6$ DP microcrystals with x varying from 0% to 1.58%. (d) XRD patterns of x% ($x = 0$ to 1.58%) Yb-doped $\text{Cs}_2\text{AgInCl}_6$ microcrystals zoomed at the peak $2\theta \sim 24.2^\circ$. No systematic shift in XRD peaks with Yb-content is observed. For comparison purpose all XRD are shifted vertically upward.

1.2.2 Optical properties of Yb-doped $\text{Cs}_2\text{AgInCl}_6$ Microcrystals:

For confirmation of Yb^{3+} incorporation in $\text{Cs}_2\text{AgInCl}_6$ microcrystal is taking place, optical properties of these microcrystals are then explored. Figure 5a shows optical absorption spectra for all the samples obtained after Kubelka–Munk transformation⁴⁴ of diffused reflectance spectra of the powder samples. A strong absorption onset at ~ 360 nm is observed for all samples corresponding to the direct band gap of $\text{Cs}_2\text{AgInCl}_6$. Below this band gap energy, a weak absorption tail is observed up to 550 nm. These observations are similar to prior reports of undoped $\text{Cs}_2\text{AgInCl}_6$ DP, where, defects in crystal gave rise to weakly absorbing tail below the optical band gap energy. However, Yb-doping does not shift sharp absorption onset ~ 360 nm which is not surprising since Yb concentration is present in small amounts in the range of 0.06 to 1.58%.

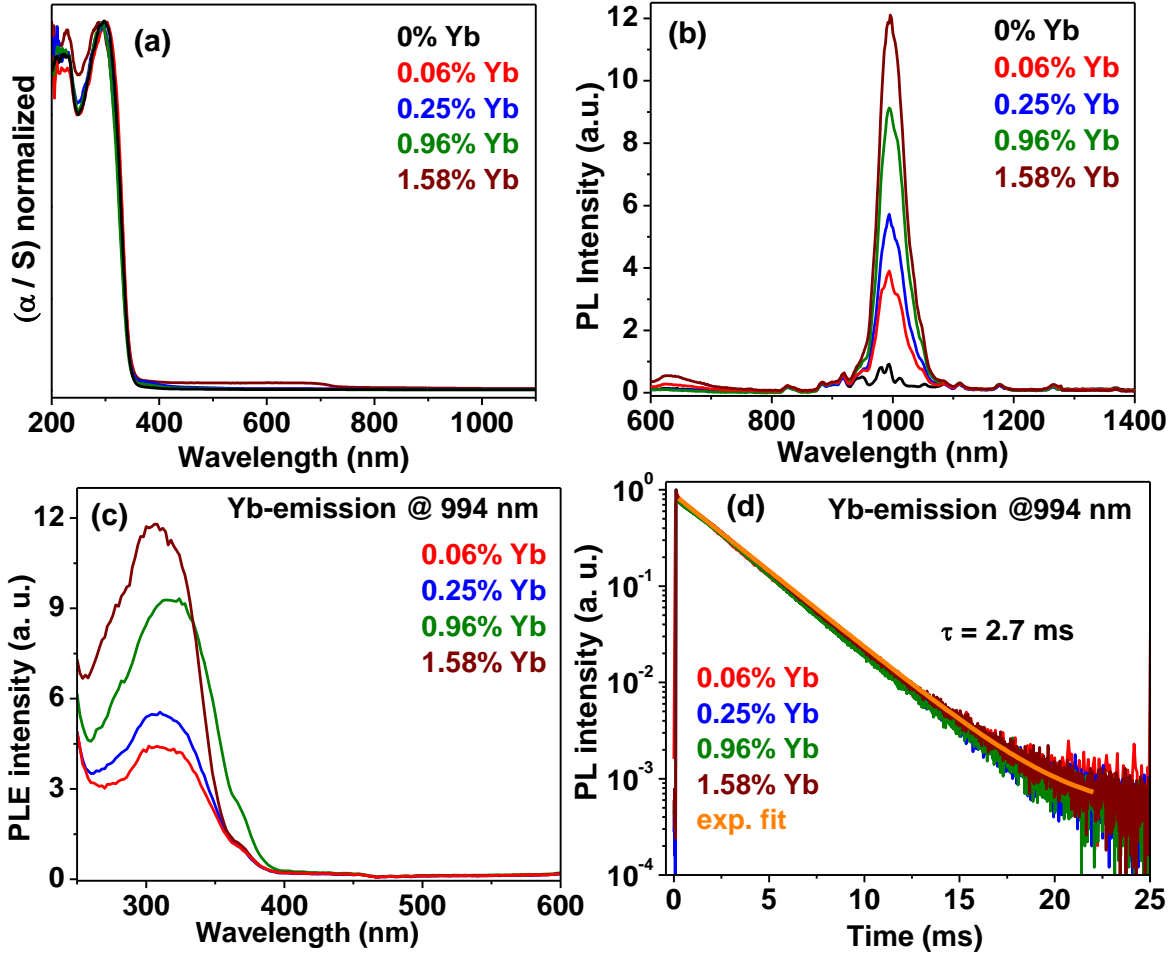


Figure 5: Optical properties of x% Yb-doped Cs₂AgInCl₆ DP microcrystals. (a) Absorption spectra (α/S) obtained through Kubelka–Munk transformation of diffused reflectance spectra, α is the absorption coefficient and S is the scattering coefficient. (b) PL spectra obtained after excitation at 300 nm. (c) PLE spectra collected for Yb-emission (~ 996 nm). (d) PL decay dynamics collected after excitation with microsecond flash lamp at 300 nm.

PL spectra in Figure 5b shows that the undoped (0% Yb) Cs₂AgInCl₆ microcrystals do not exhibit NIR emission but all the Yb doped samples shows NIR emission with peak at ~ 994 nm. Increasing the dopant concentration from 0.06% to 1.58% Yb systematically increases the intensity of this NIR emission. Figure 5a shows no new absorption channel corresponding to this NIR emission. To examine the origin of this NIR emission, PLE spectra corresponding to 994 nm emission for all Yb-doped samples are shown in Figure 5c. Clearly, the PLE spectra resemble with the absorption spectra of the host. Therefore,

the NIR Yb-emission at ~994 nm originates through excitation the host by absorption of light. The excited hosts transfer its energy to Yb dopants exciting the *f*-electrons in the dopant. The excited dopants undergoes f-f de-excitation from $^2F_{5/2} \rightarrow ^2F_{7/2}$ emitting NIR light ~994 nm.⁴⁶ There is no absorption channel in the system that overlaps with NIR Yb-emission. Therefore, the Yb-emission from Yb-doped Cs₂AgInCl₆ DPs is free from self-absorption or Forster resonance energy transfer losses. Therefore, one would expect minimum loss of Yb-emission in thin films unlike excitonic or band edge emission. Overall, the Yb doping introduced a new emission channel in NIR region unlike undoped Cs₂AgInCl₆ which is optically inactive in this region.

PL decay dynamics in Figure 5d reveals a long lifetime of 2.7 ms for Yb-emission similar to prior reports of Yb-doped CsPbCl₃ nanocrystals. All the samples show single exponential decay when excited with microsecond flash lamp. The decay profile remains very similar for all the dopant concentrations within the range of 0.06% to 1.58% Yb. This millisecond scale long lifetime is a characteristic of Yb³⁺ incorporated in the lattice. Note that surface doped Yb in tetrahedral CdSe nanocrystals show a shorter lifetime in the range of 27 μs.³⁷

1.2.3 Stability of Yb-doped Cs₂AgInCl₆ Microcrystals:

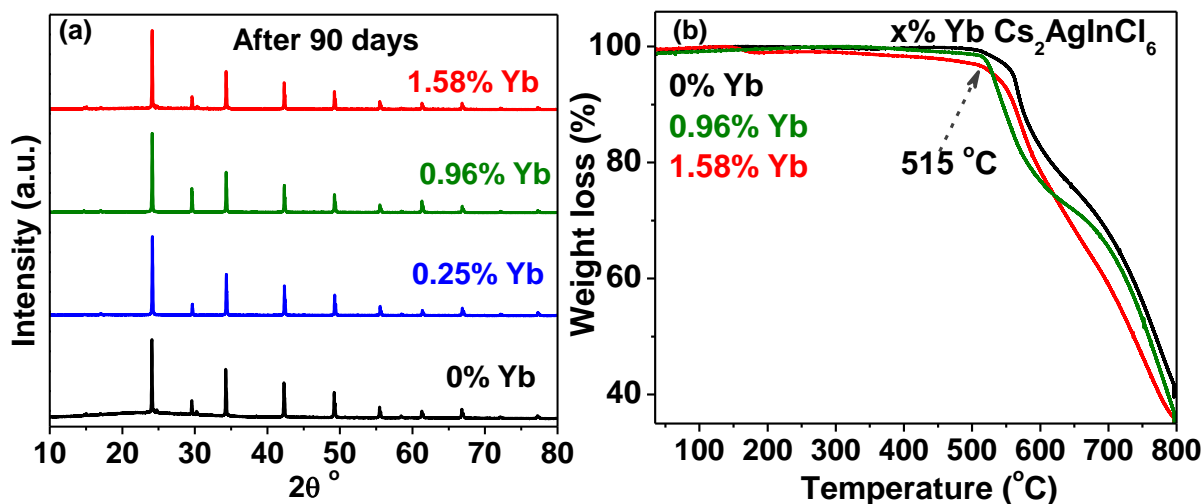


Figure 6: (a) XRD patterns. (b) TGA data for x% Yb-doped Cs₂AgInCl₆ microcrystals with different Yb-content.

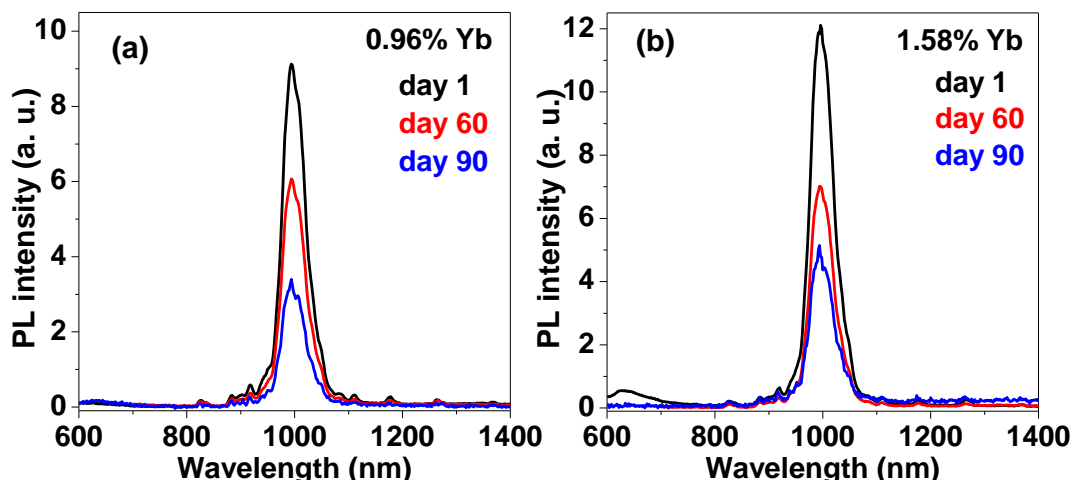


Figure 7: (a-b) PL spectra of Yb-doped $\text{Cs}_2\text{AgInCl}_6$ microcrystals recorded at different time intervals from the day of synthesis. Samples are stored in ambient conditions ($\sim 24^\circ\text{C}$, and 30% relative humidity).

In addition to above NIR optical properties, long term stability of perovskite structure and optical properties is important for real life applications. As seen in figure 6a even after storing for 90 days in ambient lab condition, the XRD pattern for different Yb doped content don't change suggesting very good stability. We then studied the thermal stability of the samples using thermogravimetric analysis as shown in figure 6b. Both the undoped and Yb-doped $\text{Cs}_2\text{AgInCl}_6$ microcrystals do not show any weight loss till $\sim 515^\circ\text{C}$ suggesting their thermal stability. However, we do seen a decrease in PL intensity of NIR Yb-emission, it decreases by ~ 3 times after 3 months compared to fresh sample on day 1, (Figure 7a and 7b). This long term stability of Yb-doped $\text{Cs}_2\text{AgInCl}_6$ DP microcrystals is notable for exploring optoelectronic devices in future.

1.3 CONCLUSIONS

Microcrystals of Yb-doped $\text{Cs}_2\text{AgInCl}_6$ are prepared. ICP-AES analysis shows only a small fraction of the added Yb concentration is present in product $\text{Cs}_2\text{AgInCl}_6$ microcrystals (0.06% to 1.58% Yb). XRD patterns suggest phase purity for all the samples. All the Yb-doped samples exhibit distinct NIR emission with peak at ~ 994 nm. Comparisons of optical absorption and PLE spectra show that both microcrystals hosts absorb the light, and subsequently transfers their energy non-radiatively to excite the Yb^{3+}

hosts. Then the de-excitation of f electrons (${}^2F_{5/2} \rightarrow {}^2F_{7/2}$ transition) of Yb^{3+} dopant results into the NIR light emission. The microcrystals exhibit a single-exponential decay of Yb-emission with a long lifetime of 2.7 ms. These Yb-doped $\text{Cs}_2\text{AgInCl}_6$ microcrystals are stable in ambient conditions making them suitable for potential applications in designing NIR light emitting diodes, and sensors.

Chapter 2: Yb-doped Cs₂AgInCl₆ Nanocrystals

2.1 METHODS

2.1.1 Chemicals:

Silver acetate (CH₃CO₂Ag, 99.99%), indium (III) acetate ((CH₃CO₂)₃In, 99.99%), ytterbium nitrate pentahydrate (Yb(NO₃)₃·5H₂O, 99.99%), cesium carbonate (Cs₂CO₃, 99%), oleic acid (90%), oleylamine (70%), benzoyl chloride (98%) and dowtherm A (eutectic mixture of 26.5% diphenyl + 73.5% diphenyl oxide) are purchased from Sigma Aldrich Chemicals. All the precursors were used without any further purification.

2.1.2 Synthesis:

2.1.2.1 Cesium Oleate Preparation:

0.5 M stock solution of cesium oleate is prepared following prior report.³⁵ Typically, Cs₂CO₃ (1630 mg) and 20 mL of oleic acid are taken into a three-neck round bottom flask (RB). The reaction mixture is degassed at 100 °C for 30 minutes and the temperature is raised to 140 °C. Once clear solution of Cs-oleate forms, the solution is stored at room temperature and requires heating up to 100 °C before use.

2.1.2.2 Synthesis of Yb-doped Cs₂AgInCl₆ Nanocrystals:

Synthesis of Yb-doped Cs₂AgInCl₆ nanocrystals were carried out by modifying prior report of synthesis of undoped Cs₂AgInCl₆ nanocrystals.³⁵ Typically, CH₃CO₂Ag (0.21 mmol, 30 mg), (CH₃CO₂)₃In (0.25 mmol, 183.5 mg), Yb(NO₃)₃·5H₂O (0.5 mmol) and 4 mL dowtherm A are taken in a 50 mL RB. The RB along with the reaction mixture is mounted on a Schlenk line apparatus. The reaction mixture is degassed by using vacuum and N₂ for about 20 minutes at 40 °C under continuous stirring. After degassing, 1 mL 0.5 M Cs-oleate stock solution (preheated at 100 °C) and 0.5 mL oleylamine is injected under N₂ flow. The 2nd round of degassing is further carried for about 15 minutes. The reaction temperature is increased to 105 °C under N₂ flow. At this set (105 °C) temperature, 250 μL benzoyl chloride dissolved in 1.8 mL degassed dowtherm A is injected quickly and the

reaction is quenched within 5s by immersing the RB in an ice-bath. $\text{Cs}_2\text{AgInCl}_6$ nanocrystals are then precipitated by centrifuging the crude mixture at 7000 rpm for 10 minutes. The supernatant is discarded and the obtained pellet is dispersed in hexane.

Similarly, synthesis of undoped $\text{Cs}_2\text{AgInCl}_6$ nanocrystals is carried out in the same way but without adding $\text{Yb}(\text{NO}_3)_3 \cdot 5\text{H}_2\text{O}$ (0.5 mmol) precursor.

2.1.3 Characterizations:

2.1.3.1 Inductively coupled plasma- Mass spectroscopy (ICP-MS):

This technique is involved in determining the elemental composition of the sample. In ICP-MS, the sample is ionized by high electron density and high temperature Argon plasma. Then the ionized sample goes to MS (mass spectrometer). MS separates elements based on the mass to charge ratio. Further, these ions are directed to electron multiplier tube detector which identifies them.

To determine the doping percentage ICP-MS analysis has been carried out using iCAP TQ ICP-MS, The Thermo Scientific instrument. All the samples were prepared in 2% HNO_3 . The concentrations of sample were kept to 20 ppb, 50 ppb, and 100 ppb. Dopant percentage was averaged out over these concentrations for accuracy.

2.1.3.2 X-ray diffraction (XRD):

Structural analysis are carried out using a Bruker D8 Advance X-ray diffraction (XRD) machine equipped with $\text{Cu K}\alpha$ (1.54 Å) radiation. Samples of thin films of nanocrystals over a glass slide are used to measure XRD pattern. Thin files of nanocrystals have prepared by drop casting of concentrated dispersion of samples.

2.1.3.3 Transmission electron microscopy (TEM) and high-resolution TEM (HRTEM):

Transmission electron microscopy (TEM) images and high-resolution TEM (HRTEM) images are captured by using a UHR FEG-TEM, JEOL JEM 2100F field emission

transmission electron microscope at 200 kV. TEM samples are prepared by drop casting a dilute dispersion of samples on carbon coated Cu TEM grid.

2.1.3.4 UV-Vis spectroscopy:

UV-Vis spectroscopy technique has been applied to know the band gap of the samples. UV-Vis spectra is the result of the light absorbed by the sample when a beam of light passes through liquid sample. When a beam of light is shines on the sample, transition of electrons happens from lower energy level to higher energy level by absorbing light of corresponding energy.

UV-visible absorption spectra of colloidal dispersion of nanocrystals are measured using Cary series UV Visible Spectrophotometers.

2.1.3.5 Steady-state PL and PL decay dynamics:

Photoluminescence (PL) is the emission of light when excited electron relaxes from excited state to ground state by radiative emission of light. The emitted light have lower in energy compare to absorbed light. Samples has been excited by using steady state Xenon lamp and steady-state PL and PL excitation spectra was obtained. In case PL decay dynamics, excitation of the sample was done by using microsecond flash lamp. In decay dynamics time correlated single photon counting are measured. All the measurements (steady-state PL, PLE and PL decay) was performed by using Edinburg FLS 980 (Edinburgh Instruments).

2.2 RESULTS AND DISCUSSION:

2.2.1 Structure and morphology of Yb-doped Cs₂AgInCl₆ Nanocrystals.

ICP-MS analysis reveals that final product nanocrystals have a 6.2% Yb. Compared to the precursor concentration (50% Yb), here again a small percentage of Yb is present in product nanocrystals, similar to the case of Yb-doping in Cs₂AgInCl₆ microcrystals. TEM and HRTEM images of undoped and Yb-doped Cs₂AgInCl₆ nanocrystals are shown in figure 8a-d. The doped nanocrystals show cubic morphology with an average edge length of nanocubes around 11.3 ± 1.7 nm (Figure 9b), compared to average edge length 10.5

± 1.7 nm for undoped nanocubes (Figure 9a). HRTEM image in Figure 8d shows single crystalline nature of nanocube with an interplanar distance of 3.7 Å and 2.6 Å corresponding to (220) and (400) planes of cubic phase of $\text{Cs}_2\text{AgInCl}_6$ DP respectively. Figure 8b shows the HRTEM of undoped $\text{Cs}_2\text{AgInCl}_6$ nanocrystals which show the crystallinity of these nanocrystals. Similar interplanar distance was observed as in Yb-doped $\text{Cs}_2\text{AgInCl}_6$ nanocrystals.

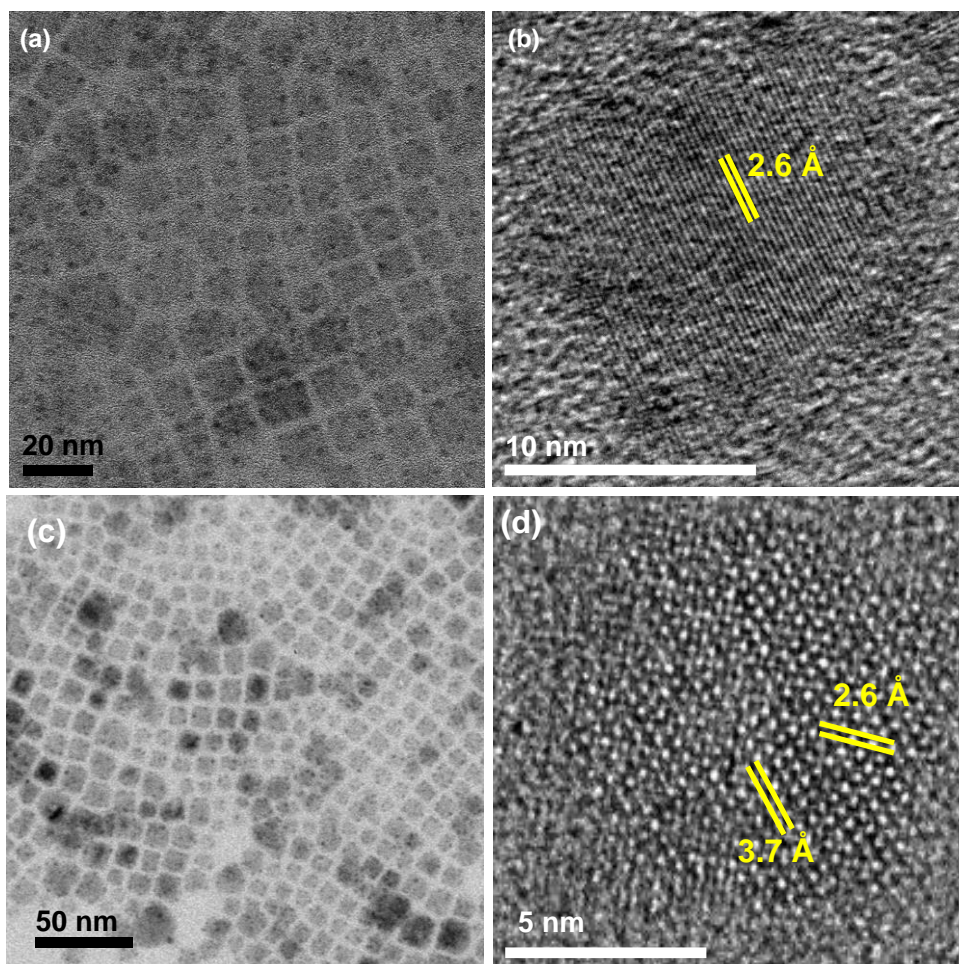


Figure 8: TEM image of (a) Undoped nanocrystals and (c) Yb-doped nanocrystals. HRTEM image of (b) Undoped and (d) Yb-doped nanocubes of each kind showing crystalline nature and respective interplanar distances.

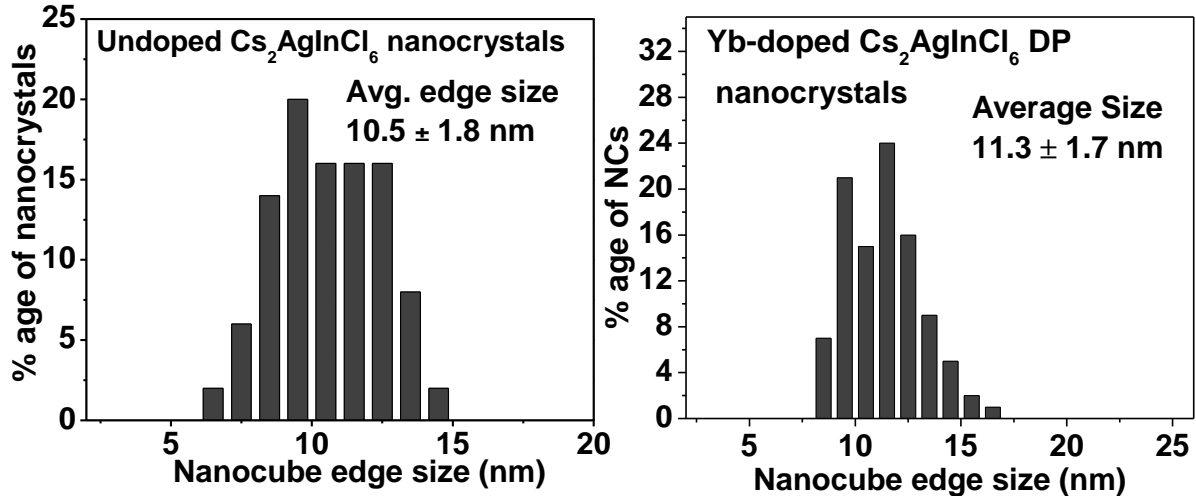


Figure 9: Size distribution histogram of (a) undoped $\text{Cs}_2\text{AgInCl}_6$ nanocrystals with average diameter of nanocube is 10.5 nm. (b) Yb-doped $\text{Cs}_2\text{AgInCl}_6$ nanocrystals with average diameter of nanocube is 11.3 nm.

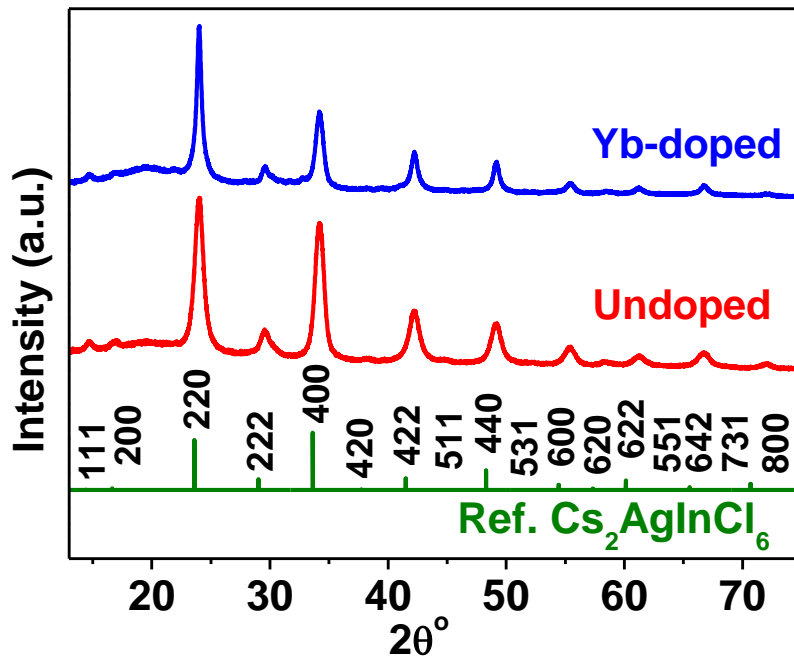


Figure 10: XRD patterns of undoped and Yb-doped nanocrystals in comparison with bulk $\text{Cs}_2\text{AgInCl}_6$ reference.

Figure 10 shows XRD patterns of both undoped and Yb-doped $\text{Cs}_2\text{AgInCl}_6$ nanocrystals in comparison with reference XRD pattern of bulk $\text{Cs}_2\text{AgInCl}_6$. Both the samples show

XRD patterns consistent with cubic phase of $\text{Cs}_2\text{AgInCl}_6$ DP with no unwanted impurity peak. XRD patterns of the undoped and 6.2% Yb-doped samples are similar with no clear shift in peaks similar to undoped and doped $\text{Cs}_2\text{AgInCl}_6$ DP microcrystals.

2.2.2 Optical properties of Yb-doped $\text{Cs}_2\text{AgInCl}_6$ nanocrystals.

Figure 11a compares the UV-visible absorption spectrum of colloidal Yb-doped $\text{Cs}_2\text{AgInCl}_6$ nanocrystals with that of undoped sample. Both undoped and Yb-doped nanocrystals show excitonic absorption at ~ 345 nm which is close to absorption onset ~ 360 nm of $\text{Cs}_2\text{AgInCl}_6$ microcrystals. This suggest that our nanocubes (edge length 11 nm) are either under weak or no quantum confinement resulting into optical band gap similar to that of bulk $\text{Cs}_2\text{AgInCl}_6$ microcrystals. Figure 11b shows comparison of PL spectra of undoped and Yb-doped $\text{Cs}_2\text{AgInCl}_6$

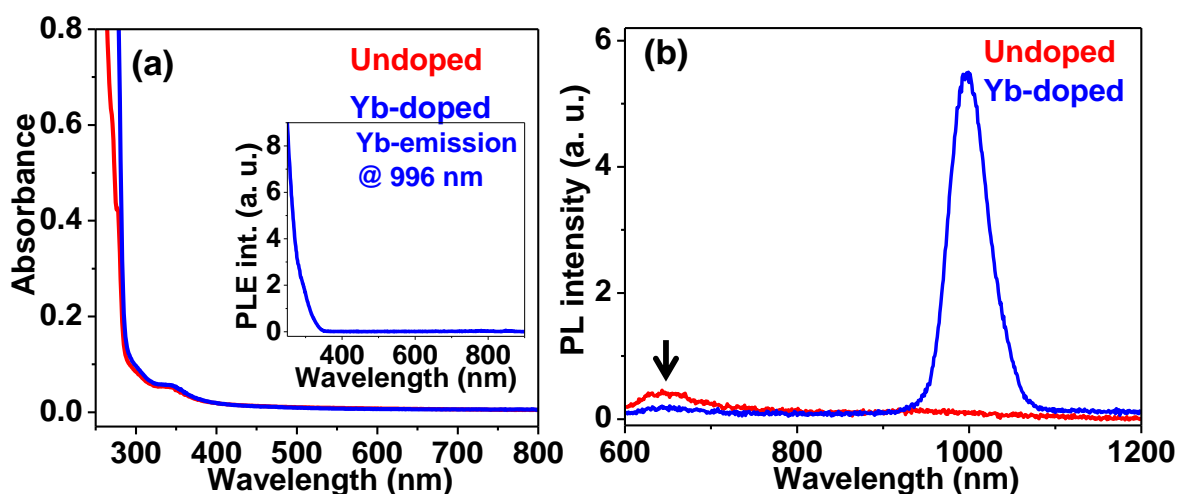


Figure 11: optical properties of undoped and 6.2% Yb-doped $\text{Cs}_2\text{AgInCl}_6$ DP nanocrystals. (a) UV-visible absorption spectra and (b) PL spectra of colloidal undoped and Yb-doped nanocrystals. PL spectra are obtained after excitation at 270 nm. Black arrow in (b) highlights weak defect induced emission in $\text{Cs}_2\text{AgInCl}_6$ DP nanocrystals. Inset of (a) shows PLE spectra collected for Yb-emission (~ 996 nm).

nanocrystals from visible to NIR region. Undoped $\text{Cs}_2\text{AgInCl}_6$ nanocrystals show weak defect related signal ~ 607 nm (see black arrow in Figure 11b) similar to prior reports of bulk $\text{Cs}_2\text{AgInCl}_6$.^{24, 30} Interestingly, Yb-doped nanocrystals show a new stronger emission

channel active in NIR region (~996 nm) unlike the undoped Cs₂AgInCl₆ nanocrystals. PLE spectra in the inset of Figure 9a resembles with the absorption spectra suggesting that the NIR Yb emission originate via photoexcitation of the host nanocrystals.

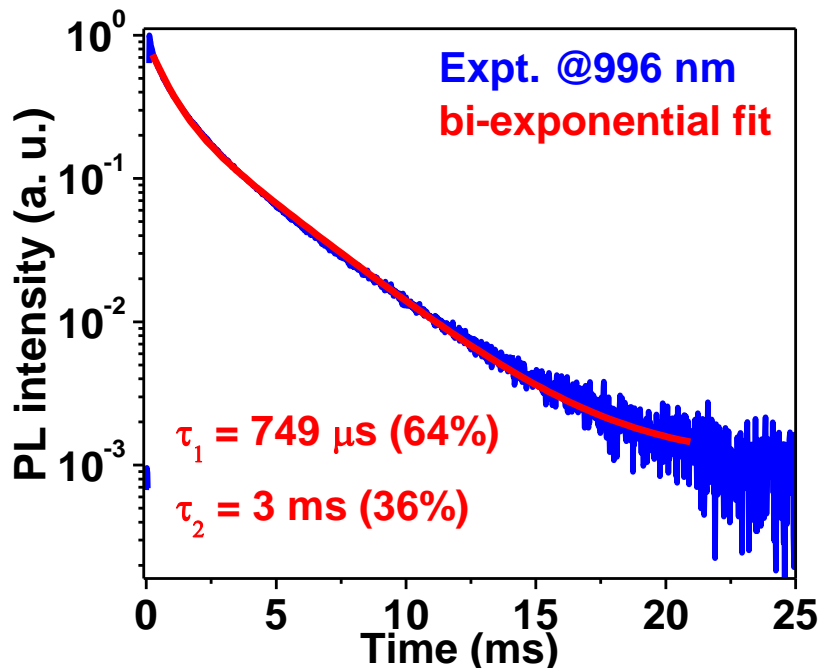


Figure 12: PL decay dynamics of Yb-emission collected at 996 nm after exciting with microsecond flash lamp at 270 nm.

PL decay dynamics in Figure 12 reveals two PL decay lifetimes, $\tau_1 = 3 \text{ ms}$ (36% contribution) and short component $\tau_2 = 749 \mu\text{s}$ (64% contribution) for the Yb-emission at 996 nm. The longer component 3 ms lifetime of nanocrystals is close to the 2.7 ms lifetime for Yb-doped Cs₂AgInCl₆ microcrystals (Figure 5d). Probably the shorter (749 μs) lifetime is attributed to Yb dopants with slightly distorted coordination near the surface.

2.3 CONCLUSIONS

Colloidal nanocrystals of Yb-doped Cs₂AgInCl₆ are prepared. ICP-MS analysis shows only a small fraction of the added Yb concentration is present in product Cs₂AgInCl₆ nanocrystals (6.2% Yb). XRD patterns suggest phase purity for all the samples. All the

Yb-doped samples exhibit distinct NIR emission with peak at ~994 nm. Comparisons of optical absorption and PLE spectra show that both microcrystals and nanocrystals hosts absorb the light, and subsequently transfers their energy non-radiatively to excite the Yb³⁺ hosts. Then the de-excitation of *f* electrons ($^2F_{5/2} \rightarrow ^2F_{7/2}$ transition) of Yb³⁺ dopant results into the NIR light emission. Nanocrystals show somewhat different PL decay profile with bi-exponential decay for Yb-emission with contribution from 3 ms (36 %) and 749 μ s (64%) lifetimes. These Yb-doped Cs₂AgInCl₆ nanocrystals are stable in ambient conditions making them suitable for potential applications in designing NIR light emitting diodes, and sensors.

REFERENCES

- 1) Stranks, S. D.; Snaith, H. J. Metal-Halide Perovskites for Photovoltaic and Light-Emitting Devices. *Nat. Nanotechnol.* **2015**, *10*, 391.
- 2) Protesescu, L.; Yakunin, S.; Bodnarchuk, M. I.; Krieg, F.; Caputo, R.; Hendon, C. H.; Yang, R. X.; Walsh, A.; Kovalenko, M. V. Nanocrystals of Cesium Lead Halide Perovskites (CsPbX₃, X = Cl, Br, and I): Novel Optoelectronic Materials Showing Bright Emission with Wide Color Gamut. *Nano Lett.* **2015**, *15*, 3692-3696.
- 3) Swarnkar, A.; Chulliyil, R.; Ravi, V. K.; Irfanullah, M.; Chowdhury, A.; Nag, A. Colloidal CsPbBr₃ Perovskite Nanocrystals: Luminescence Beyond Traditional Quantum Dots. *Angew. Chem., Int. Ed.* **2015**, *54*, 15424-15428.
- 4) Swarnkar, A.; Marshall, A. R.; Sanehira, E. M.; Chernomordik, B. D.; Moore, D. T.; Christians, J. A.; Chakrabarti, T.; Luther, J. M. Quantum Dot-Induced Phase Stabilization of α -CsPbI₃ Perovskite for High-Efficiency Photovoltaics. *Science* **2016**, *354*, 92-95.
- 5) Ramasamy, P.; Lim, D.-H.; Kim, B.; Lee, S.-H.; Lee, M.-S.; Lee, J.-S. All-Inorganic Cesium Lead Halide Perovskite Nanocrystals for Photodetector Applications. *Chem. Commun.* **2016**, *52*, 2067-2070.
- 6) Sanehira, E. M.; Marshall, A. R.; Christians, J. A.; Harvey, S. P.; Ciesielski, P. N.; Wheeler, L. M.; Schulz, P.; Lin, L. Y.; Beard, M. C.; Luther, J. M. Enhanced Mobility CsPbI₃ Quantum Dot Arrays for Record-Efficiency, High-Voltage Photovoltaic Cells. *Sci. Adv.* **2017**, *3*, eaao4204.
- 7) Lin, K.; Xing, J.; Quan, L. N.; de Arquer, F. P. G.; Gong, X.; Lu, J.; Xie, L.; Zhao, W.; Zhang, D.; Yan, C.; et al. Perovskite Light-Emitting Diodes with External Quantum Efficiency Exceeding 20 Per Cent. *Nature* **2018**, *562*, 245-248.

- 8) Chiba, T.; Hayashi, Y.; Ebe, H.; Hoshi, K.; Sato, J.; Sato, S.; Pu, Y.-J.; Ohisa, S.; Kido, J. Anion-Exchange Red Perovskite Quantum Dots with Ammonium Iodine Salts for Highly Efficient Light-Emitting Devices. *Nat. Photonics* **2018**, *12*, 681-687.
- 9) Tong, Y.; Fu, M.; Bladt, E.; Huang, H.; Richter, A. F.; Wang, K.; Müller-Buschbaum, P.; Bals, S.; Tamarat, P.; Lounis, B.; et al. Chemical Cutting of Perovskite Nanowires into Single-Photon Emissive Low-Aspect-Ratio CsPbX₃ (X=Cl, Br, I) Nanorods. *Angew. Chem., Int. Ed.* **2018**, *130*, 16094-16098.
- 10) Kumar, G. S.; Pradhan, B.; Kamilya, T.; Acharya, S. Enhancing Performances of Hybrid Perovskite Light Emitting Diodes with Thickness Controlled PMMA Interlayer. *Bull. Chem. Soc. Jpn.* **2018**, *91*, 1241-1248.
- 11) Song, J.; Fang, T.; Li, J.; Xu, L.; Zhang, F.; Han, B.; Shan, Q.; Zeng, H. Organic–Inorganic Hybrid Passivation Enables Perovskite QLEDs with an EQE of 16.48%. *Adv. Mater.* **2018**, *30*, 1805409.
- 12) Liu, L.; Deng, L.; Huang, S.; Zhang, P.; Linnros, J.; Zhong, H.; Sychugov, I. Photodegradation of Organometal Hybrid Perovskite Nanocrystals: Clarifying the Role of Oxygen by Single-Dot Photoluminescence. *J. Phys. Chem. Lett.* **2019**, *10*, 864-869.
- 13) Mondal, N.; De, A.; Samanta, A. Achieving near-Unity Photoluminescence Efficiency for Blue-Violet-Emitting Perovskite Nanocrystals. *ACS Energy Lett.* **2019**, *4*, 32-39.
- 14) Juarez-Perez, E. J.; Hawash, Z.; Raga, S. R.; Ono, L. K.; Qi, Y. Thermal Degradation of CH₃NH₃PbI₃ Perovskite into NH₃ and CH₃I Gases Observed by Coupled Thermogravimetry–Mass Spectrometry Analysis. *Energy Environ. Sci.* **2016**, *9*, 3406-3410.
- 15) Swarnkar, A.; Mir, W. J.; Nag, A. Can B-Site Doping or Alloying Improve Thermal- and Phase-Stability of All-Inorganic CsPbX₃ (X = Cl, Br, I) Perovskites? *ACS Energy Lett.* **2018**, *3*, 286-289.
- 16) Wei, Y.; Cheng, Z.; Lin, J. An Overview on Enhancing the Stability of Lead Halide Perovskite Quantum Dots and Their Applications in Phosphor-Converted LEDs. *Chem. Soc. Rev.* **2019**, *48*, 310-350.
- 17) Noel, N. K.; Stranks, S. D.; Abate, A.; Wehrenfennig, C.; Guarnera, S.; Haghighirad, A.-A.; Sadhanala, A.; Eperon, G. E.; Pathak, S. K.; Johnston, M. B.; et al. Lead-Free Organic–Inorganic Tin Halide Perovskites for Photovoltaic Applications. *Energy Environ. Sci.* **2014**, *7*, 3061-3068.
- 18) Hao, F.; Stoumpos, C. C.; Cao, D. H.; Chang, R. P. H.; Kanatzidis, M. G. Lead-free Solid-state Organic-inorganic Halide Perovskite Solar Cells. *Nat. Photonics*, **2014**, *8*, 489-494.
- 19) Kumar, M. H.; Dharani, S.; Leong, W. L.; Boix, P. P.; Prabhakar, R. R.; Baikie, T.; Shi, C.; Ding, H.; Ramesh, R.; Asta, M.; et al. Leadfree halide perovskite solar cells

- with high photocurrents realized through vacancy modulation. *Adv. Mater.* 2014, 26, 7122–7127
- 20) Ju, M.-G.; Dai, J.; Ma, L.; Zeng, X. C. Lead-free mixed tin and germanium perovskites for photovoltaic application. *J. Am. Chem. Soc.* **2017**, 139, 8038–8043.
 - 21) Park, B.; Philippe, B.; Zhang, X.; Rensmo, H.; Boschloo, G.; Johansson, E. M. J. Bismuth based hybrid perovskites $A_3Bi_2I_9$ (A: methylammonium or cesium) for solar cell application. *Adv. Mater.* **2015**, 27, 6806–6813
 - 22) Saparov, B.; Hong, F.; Sun, J.-P.; Duan, H.-S.; Meng, W.; Cameron, S.; Hill, I. G.; Yan, Y.; Mitzi, D. B. Thin-film preparation and characterization of $Cs_3Sb_2I_9$: A lead-free layered perovskite semiconductor. *Chem. Mater.* **2015**, 27, 5622–5632.
 - 23) Pal, J.; Manna, S.; Mondal, A.; Das, S.; Adarsh, K. V.; Nag, A. Colloidal Synthesis and Photophysics of $M_3Sb_2I_9$ (M = Cs and Rb) Nanocrystals: Lead-Free Perovskites. *Angew. Chem., Int. Ed.* **2017**, 56, 14187–14191.
 - 24) Volonakis, G.; Haghghirad, A. A.; Milot, R. L.; Sio, W. H.; Filip, M. R.; Wenger, B.; Johnston, M. B.; Herz, L. M.; Snaith, H. J.; Giustino, F. $Cs_2InAgCl_6$: A new lead-free halide double perovskite with direct band gap. *J. Phys. Chem. Lett.* **2017**, 8, 772–778
 - 25) Zhou, J.; Xia, Z.; Molokeev, M. S.; Zhang, X.; Peng, D.; Liu, Q. Composition design, optical gap and stability investigations of lead-free halide double perovskite $Cs_2AgInCl_6$. *J. Mater. Chem. A* **2017**, 5, 15031–15037.
 - 26) Slavney, A. H.; Hu, T.; Lindenberg, A. M.; Karunadasa, H. I. A Bismuth-Halide Double Perovskite with Long Carrier Recombination Lifetime for Photovoltaic Applications. *J. Am. Chem. Soc.* **2016**, 138, 2138–2141.
 - 27) Zhao, X.-G.; Yang, J.-H.; Fu, Y.; Yang, D.; Xu, Q.; Yu, L.; Wei, S.-H.; Zhang, L. Design of Lead-Free Inorganic Halide Perovskites for Solar Cells Via Cation-Transmutation. *J. Am. Chem. Soc.* **2017**, 139, 2630–2638.
 - 28) Meng, W.; Wang, X.; Xiao, Z.; Wang, J.; Mitzi, D. B.; Yan, Y. Parity-Forbidden Transitions and Their Impact on the Optical Absorption Properties of Lead-Free Metal Halide Perovskites and Double Perovskites. *J. Phys. Chem. Lett.* **2017**, 8, 2999–3007.
 - 29) Ravi, V. K.; Singhal, N.; Nag, A. Initiation and Future Prospects of Colloidal Metal Halide Double-Perovskite Nanocrystals: Cs_2AgBiX_6 (X = Cl, Br, I). *J. Mater. Chem. A* **2018**, 6, 21666–21675.
 - 30) Luo, J.; Li, S.; Wu, H.; Zhou, Y.; Li, Y.; Liu, J.; Li, J.; Li, K.; Yi, F.; Niu, G.; et al. $Cs_2AgInCl_6$ Double Perovskite Single Crystals: Parity Forbidden Transitions and Their Application for Sensitive and Fast UV Photodetectors. *ACS Photonics* **2018**, 5, 398–405.

- 31) Connor, B. A.; Leppert, L.; Smith, M. D.; Neaton, J. B.; Karunadasa, H. I. Layered Halide Double Perovskites: Dimensional Reduction of Cs₂AgBiBr₆. *J. Am. Chem. Soc.* **2018**, *140*, 5235-5240.
- 32) Sarkar, A.; Acharyya, P.; Sasmal, R.; Pal, P.; Agasti, S. S.; Biswas, K. Synthesis of Ultrathin Few-Layer 2D Nanoplates of Halide Perovskite Cs₃Bi₂I₉ and Single-Nanoplate Super-Resolved Fluorescence Microscopy. *Inorg. Chem.* **2018**, *57*, 15558-15565.
- 33) Tran, T. T.; Panella, J. R.; Chamorro, J. R.; Morey, J. R.; McQueen, T. M. *Mater. Horiz.* **2017**, *4*, 688–693
- 34) K, N. N.; Nag, A. Synthesis and Luminescence of Mn-Doped Cs₂AgInCl₆ Double Perovskites. *Chem. Commun.* **2018**, *54*, 5205-5208
- 35) Locardi, F.; Cirignano, M.; Baranov, D.; Dang, Z.; Prato, M.; Drago, F.; Ferretti, M.; Pinchetti, V.; Fanciulli, M.; Brovelli, S.; et al. Colloidal Synthesis of Double Perovskite Cs₂AgInCl₆ and Mn-Doped Cs₂AgInCl₆ Nanocrystals. *J. Am. Chem. Soc.* **2018**, *140*, 12989-12995.
- 36) Bol, A. A.; van Beek, R.; Meijerink, A. On the Incorporation of Trivalent Rare Earth Ions in II–VI Semiconductor Nanocrystals. *Chem. Mater.* **2002**, *14*, 1121-1126.
- 37) Martín-Rodríguez, R.; Geitenbeek, R.; Meijerink, A. Incorporation and Luminescence of Yb³⁺ in CdSe Nanocrystals. *J. Am. Chem. Soc.* **2013**, *135*, 13668-13671.
- 38) Creutz, S. E.; Fainblat, R.; Kim, Y.; De Siena, M. C.; Gamelin, D. R. A Selective Cation Exchange Strategy for the Synthesis of Colloidal Yb³⁺-Doped Chalcogenide Nanocrystals with Strong Broadband Visible Absorption and Long-Lived near-Infrared Emission. *J. Am. Chem. Soc.* **2017**, *139*, 11814-11824.
- 39) Pan, G.; Bai, X.; Yang, D.; Chen, X.; Jing, P.; Qu, S.; Zhang, L.; Zhou, D.; Zhu, J.; Xu, W.; et al. Doping Lanthanide into Perovskite Nanocrystals: Highly Improved and Expanded Optical Properties. *Nano Lett.* **2017**, *17*, 8005-8011.
- 40) Milstein, T. J.; Kroupa, D. M.; Gamelin, D. R. Picosecond Quantum Cutting Generates Photoluminescence Quantum Yields over 100% in Ytterbium-Doped CsPbCl₃ Nanocrystals. *Nano Lett.* **2018**, *18*, 3792-3799.
- 41) Mir, W. J.; Mahor, Y.; Lohar, A.; Jagadeeswararao, M.; Das, S.; Mahamuni, S.; Nag, A. Postsynthesis Doping of Mn and Yb into CsPbX₃ (X = Cl, Br, or I) Perovskite Nanocrystals for Downconversion Emission. *Chem. Mater.* **2018**, *30*, 8170-8178.
- 42) Luo, X.; Ding, T.; Liu, X.; Liu, Y.; Wu, K. Quantum-Cutting Luminescent Solar Concentrators Using Ytterbium-Doped Perovskite Nanocrystals. *Nano Lett.* **2019**, *19*, 338-341.
- 43) Wang, F.; Liu, X. Recent Advances in the Chemistry of Lanthanide-Doped Upconversion Nanocrystals. *Chem. Soc. Rev.* **2009**, *38*, 976-989.

- 44) Shanon Database of Ionic Radii. <http://abulafia.mt.ic.ac.uk/shannon/ptable.php> (2019).
- 45) Eickhoff, T.; Grosse, P.; Theiss, W. Diffuse Reflectance Spectroscopy of Powders. *Vib. Spectrosc.* **1990**, *1*, 229-233.
- 46) Sontakke, A. D.; Annapurna, K. Phonon Assisted Effective Non-Resonant Energy Transfer Based 1 μm Luminescence from Nd^{3+} - Yb^{3+} Codoped Zinc-Boro-Bismuthate Glasses. *J. Lumin.* **2013**, *138*, 229-234.



Note: Copyright.com supplies permissions but not the copyrighted content itself.

1
PAYMENT

2
REVIEW

3
CONFIRMATION

Step 3: Order Confirmation

Thank you for your order! A confirmation for your order will be sent to your account email address. If you have questions about your order, you can call us 24 hrs/day, M-F at +1.855.239.3415 Toll Free, or write to us at info@copyright.com. This is not an invoice.

Confirmation Number: 11800296
Order Date: 03/20/2019

If you paid by credit card, your order will be finalized and your card will be charged within 24 hours. If you choose to be invoiced, you can change or cancel your order until the invoice is generated.

Payment Information

Yogesh Mahor
Indisn institute of Science Education and
Research Pune
yogesh.mahor@students.iiserpune.ac.in
+91 25908464
Payment Method: n/a

Order Details

Journal of materials chemistry. A, Materials for energy and sustainability

Order detail ID: 71856210
Order License Id: 4553121089648
ISSN: 2050-7496
Publication Type: e-Journal
Volume:
Issue:
Start page:
Publisher: Royal Society of Chemistry
Author/Editor: Royal Society of Chemistry (Great Britain)

Permission Status: **Granted**

Permission type: Republish or display content
Type of use: Thesis/Dissertation

Requestor type Academic institution

Format Print, Electronic

Portion chart/graph/table/figure

Number of charts/graphs/tables/figures 1

The requesting person/organization yogesh mahor

Title or numeric reference of the portion(s)

Fig. 1 (a) Transformation of lead halide perovskites to halide DPs by replacement of two Pb²⁺ cations with M³⁺ and M⁺ cations each. (b) Summary of the aspects of DP NCs discussed here.

Title of the article or chapter the portion is from	Initiation and future prospects of colloidal metal halide double-perovskite nanocrystals: Cs ₂ AgBiX ₆ (X = ¼ Cl, Br, I)
Editor of portion(s)	n/a
Author of portion(s)	n/a
Volume of serial or monograph	n/a
Issue, if republishing an article from a serial	6
Page range of portion	21668
Publication date of portion	2 aug 2018
Rights for	Main product and any product related to main product
Duration of use	Life of current edition
Creation of copies for the disabled	no
With minor editing privileges	yes
For distribution to	Worldwide
In the following language(s)	Original language of publication
With incidental promotional use	no
Lifetime unit quantity of new product	Up to 499
Title	Yb-Doped Cs ₂ AgInCl ₆ Double Perovskite microcrystals and nanocrystals
Institution name	IISER Pune
Expected presentation date	May 2019

Note: This item will be invoiced or charged separately through CCC's **RightsLink** service. [More info](#)

\$ 0.00

Total order items: 1

This is not an invoice.

Order Total: 0.00 USD